Testing velocity-dependent *CPT*-violating gravitational forces with radio pulsars

Lijing Shao^{1,2,*} and Quentin G. Bailey^{3,†}

¹Kavli Institute for Astronomy and Astrophysics, Peking University, Beijing 100871, China ²Max-Planck-Institut für Radioastronomie, Auf dem Hügel 69, D-53121 Bonn, Germany ³Department of Physics and Astronomy, Embry-Riddle Aeronautical University, Prescott, Arizona 86301, USA

(Received 17 September 2018; published 29 October 2018)

In the spirit of effective field theory, the standard-model extension (SME) provides a comprehensive framework to systematically probe the possibility of Lorentz/CPT violation. In the pure gravity sector, operators with mass dimension larger than 4, while in general being advantageous to short-range experiments, are hard to investigate with systems of astronomical size. However, there is exception if the leading-order effects are CPT-violating and velocity-dependent. Here we study the lowest-order operators in the pure gravity sector that violate the CPT symmetry with carefully chosen relativistic binary pulsar systems. Applying the existing analytical results to the dynamics of a binary orbit, we put constraints on various coefficients for Lorentz/CPT violation with mass dimension 5. These constraints, being derived from the post-Newtonian dynamics for the first time, are complementary to those obtained from the kinematics in the propagation of gravitational waves.

DOI: 10.1103/PhysRevD.98.084049

I. INTRODUCTION

There is a great deal of theoretical interest to probe new physics beyond the standard model of particle physics, and the general relativity (GR) theory of gravitation [1–4]. Most of them stem from the need for a theory of quantum gravity, namely, to unify quantum field theories and GR, or in other words, to describe the four fundamental forces within a single mathematical setting [5–7]. Up to now, although there are achievements at different levels, not one proposal has been singled out as the widely accepted final theory for quantum gravity. On the other hand, observational evidence that was accumulated during the past decades—with intriguing puzzles from dark matter, dark energy, and inflationary cosmology, just to name a few—points to the need going beyond the current paradigm of modern theoretical physics [8–10].

Broadly speaking, there are two ways to investigate new physics beyond our current understanding: theory specific and theory agnostic. Effective field theory (EFT) is a natural candidate framework for the latter [6,11]. In the spirit of EFT, Kostelecký and collaborators have developed a comprehensive framework, dubbed the standard-model extension (SME), to catalogue all possible operators that are gauge invariant, Lorentz covariant, and energy-momentum conserving [5,12–17]. In general, a violation in *CPT* implies

a violation in the Lorentz symmetry [18]. In a practical way, we will collectively call the coefficients of new operators beyond the standard model and GR *coefficients for Lorentz/CPT violation* [19]. During the past decades, the SME has been successfully applied in various experiments, and many constraints were set on the coefficients for Lorentz/*CPT* violation [19–21]. No statistically convincing violation has been found yet [19].

We here focus on the pure gravity sector of SME [14,15,17,22–25]. The general framework for Riemann-Cartan spacetime was described in Ref. [14]. To be mathematically compatible with the Riemann-Cartan geometry, Lorentz/CPT breaking can be considered to be spontaneous, instead of explicit [26]. Extra dynamical fields in the framework obtain their vacuum expectation values through symmetry breaking cosmologically, in analog with the Higgs mechanism in the standard model. However in SME these fields are not necessarily to be scalar fields, but can take on nontrivial spacetime indices and therefore have tensorial nature. Therefore, after symmetry breaking, the effective Lagrangian is observer Lorentz invariant, but particle Lorentz violating [10,14,15]. To be fully compatible with geometrical requirements at desired orders, the underlying fluctuating Nambu-Goldstone modes that arise from the symmetry breaking need to be properly accounted for [14,15]. In Ref. [15] the post-Newtonian behaviors from the pure-gravity sector of SME for operators with mass dimension up to 4 were studied. The leading-order post-Newtonian effects are described by a tensor field, $\bar{s}^{\mu\nu}$, where the "bar"

lshao@pku.edu.cn baileyq@erau.edu

indicates that it is the vacuum expectation value of the underlying dynamical field $s^{\mu\nu}$. Different experiments, including lunar laser ranging [27,28], atom interferometers [29–31], cosmic rays [32], pulsar timing [33–38], planetary orbital dynamics [39], and gravitational waves [40,41] were used to constrain $\bar{s}^{\mu\nu}$ (see Hees *et al.* [20] for a review).

Recently, higher-dimensional operators with mass dimension larger than 4 in the gravity sector of SME were investigated, and short-range gravity experiments in laboratory were identified to be the best to constrain these terms due to the extra powers in 1/r for the gravitational forces derived from these operators [22,23,42,43]. However, there is an exception. Bailey and Havert [25] found that the leading-order CPT-violating operators with mass dimension 5 produce a gravitational force, between two objects a and b, proportional to $(v_a - v_b)/r^3$. For short-range gravity experiments, $(v_a - v_b)/c$ is very close to zero, thus these experiments are very hard, if ever possible, to probe these terms. Estimated sensitivities of different experiments to these new operators were tabulated (see Table III in Ref. [25]), where binary pulsars turn out to be among the most sensitive probes. This motivates us to take a closer look at these new operators, and to collect the best binary pulsars in order to derive constraints on the coefficients for Lorentz/CPT violation.

The paper is organized as follows. In the next section, we review the structure of the gravity sector of SME at leading orders, and give the expressions for secular changes for elements of a binary orbit [15,25]. Then in Sec. III we carefully choose the binary pulsars that are suitable for the test, and discuss our approach to evade difficulties related to observationally unknown angles and the consistency in using timing parameters with a priori unknown component masses. Our direct constraints are summarised in Table IV, and they are properly converted to constraints on the coefficients in the Lagrangian in Tables V and VI. In the last section we point out the perturbative nature of SME and the post-Newtonian approach, thus we should keep caveats in mind when dealing with strongly self-gravitating bodies like neutron stars (NSs) [44,45]. Throughout the paper, unless explicitly stated, we use units where $\hbar = c = 1$.

II. THEORY

At present there are two approaches to the gravity sector of the SME. The first is a general coordinate invariant version [14], while the second focuses on a spacetime that can be expanded around a Minkowski metric [17]. These two approaches have distinct underlying methodology, but are interrelated. We use the latter in this work. We restrict ourselves to the discussion of the part of spacetime where, after fixing the gauge (say, the harmonic gauge), linearized gravity is a good approximation. The metric is decomposed into a flat-spacetime metric, $\eta_{\mu\nu} \equiv \text{diag}\{-,+,+,+\}$, and a perturbation, $h_{\mu\nu}$,

$$g_{\mu\nu} = \eta_{\mu\nu} + h_{\mu\nu},\tag{1}$$

where $|h_{\mu\nu}| \ll 1$. With this assumption, it is possible to write down the generic Lagrangian density for a spin-2 massless particle, organized by the order of the mass dimension of the coupling coefficients [14,15,25,42,46],

$$\mathcal{L} = \mathcal{L}_{GR} + \mathcal{L}_{SME}^{(4)} + \mathcal{L}_{SME}^{(5)} + \cdots, \tag{2}$$

where the GR terms are,

$$\mathcal{L}_{GR} = -\frac{1}{32\pi G} h^{\mu\nu} G_{\mu\nu} + \frac{1}{2} h_{\mu\nu} T^{\mu\nu}_{\text{matter}}, \tag{3}$$

with $G_{\mu\nu}$ the linearized Einstein tensor, and $T^{\mu\nu}_{\rm matter}$ the matters' energy-momentum tensor.

The leading-order corrections in Eq. (2) are [25],

$$\mathcal{L}_{\text{SME}}^{(4)} = \frac{1}{32\pi G} \bar{s}^{\mu\kappa} h^{\nu\lambda} \mathcal{G}_{\mu\nu\kappa\lambda},\tag{4}$$

$$\mathcal{L}_{\mathrm{SME}}^{(5)} = -\frac{1}{128\pi G} h_{\mu\nu} q^{\mu\rho\alpha\nu\beta\sigma\gamma} \partial_{\beta} R_{\rho\alpha\sigma\gamma}, \tag{5}$$

where $R_{\rho\alpha\sigma\gamma}$ is the linearized Riemann curvature tensor, and $\mathcal{G}_{\mu\nu\kappa\lambda}$ is its double dual; $\bar{s}^{\mu\kappa}$ and $q^{\mu\rho\alpha\nu\beta\sigma\gamma}$ are coefficients for Lorentz/CPT violation. Components of $\bar{s}^{\mu\kappa}$ are dimensionless, while those of $q^{\mu\rho\alpha\nu\beta\sigma\gamma}$ have the dimension of the length (or the inverse mass). In the operational counting in SME [14], $\mathcal{L}_{SME}^{(4)}$ breaks the Lorentz symmetry, but preserves the CPT symmetry, while $\mathcal{L}_{\mathrm{SME}}^{(5)}$ breaks both Lorentz and CPT symmetries [14]. $\bar{s}^{\mu\kappa}$ is a symmetric, traceless tensor, thus it has 9 independent components. The first three indices of $q^{\mu\rho\alpha\nu\beta\sigma\gamma}$ are completely antisymmetric, while the last four have the symmetry of the Riemann tensor. Thus, there are 60 independent coefficients in $q^{\mu\rho\alpha\nu\beta\sigma\gamma}$ [25,46]. Because $\bar{s}^{\mu\kappa}$ has already been discussed in various literature [14,15,19], we will focus on $q^{\mu\rho\alpha\nu\beta\sigma\gamma}$ in this paper. The contributions from $\bar{s}^{\mu\kappa}$ are kept in some expressions in the text, only for interested readers for convenient comparisons; all numerical calculations in this paper have set $\bar{s}^{\mu\kappa} = 0$. As mentioned by Bailey and Havert [25], some specific models have direct or indirect mappings to the Lagrangian in Eqs. (4) and (5), like the vector field models with a potential term driving spontaneous Lorentz/ diffeomorphism breaking [47] and those with additional beyond-Maxwell kinetic terms [48], noncommutative geometry [49], quantum gravity [50], and so on.

Neglecting higher-order terms, the field equation derived from Eq. (2) reads [25],

$$G^{\mu\nu} = 8\pi G T^{\mu\nu}_{\rm matter} + \bar{s}_{\kappa\lambda} \mathcal{G}^{\mu\kappa\nu\lambda} - \frac{1}{4} q^{\rho\alpha(\mu\nu)\beta\sigma\gamma} \partial_{\beta} R_{\rho\alpha\sigma\gamma}, \qquad (6)$$

where (\cdot) denotes the symmetrization of indices.

With post-Newtonian techniques [51], one can derive the leading-order Lagrangian for two bodies a and b [15,25],

$$L = \frac{1}{2} (m_a v_a^2 + m_b v_b^2) + \frac{G m_a m_b}{r} \left(1 + \frac{3}{2} \bar{s}_{00} + \frac{1}{2} \bar{s}_{jk} \hat{n}^j \hat{n}^k \right)$$

$$+ \frac{G m_a m_b}{2r} [3 \bar{s}_{0j} (v_a^j + v_b^j) + \bar{s}_{0j} \hat{n}^j (v_a^k + v_b^k) \hat{n}^k]$$

$$- \frac{3G m_a m_b}{2r^2} v_{ab}^j (K_{jklm} \hat{n}^k \hat{n}^l \hat{n}^m - K_{jkkl} \hat{n}^l),$$
(7)

where m_a and m_b are masses, v_a and v_b are velocities (a boldface indicates vectors), $\mathbf{r} \equiv \mathbf{r}_a - \mathbf{r}_b$ is the relative separation, and $\hat{\mathbf{n}} \equiv \mathbf{r}/r$ with $r \equiv |\mathbf{r}|$, $v_{ab} \equiv v_a - v_b$. As can be seen from the second line of the equation, while the $\bar{s}^{\mu\nu}$ terms depend on the "absolute" velocities of bodies, the K_{jklm} terms (to be introduced below) only depend on the relative velocity of two bodies. When $\bar{s}^{\mu\nu} = 0$, the Lagrangian reduces to,

$$L = \frac{1}{2} (m_a v_a^2 + m_b v_b^2) + \frac{G m_a m_b}{r} - \frac{3G m_a m_b}{2r^2} v_{ab}^j (K_{jklm} \hat{n}^k \hat{n}^l \hat{n}^m - K_{jkkl} \hat{n}^l).$$
 (8)

In Eq. (7) we have defined,

$$K_{jklm} \equiv -\frac{1}{6} (q_{0jk0l0m} + q_{n0knljm} + q_{njknl0m} + \text{permutations}),$$
(9)

which is the linear combination of $q^{\mu\rho\alpha\nu\beta\sigma\gamma}$ that enters the post-Newtonian scheme at leading order [25]; "permutations" here mean all symmetric permutations in the last three indices klm. While the post-Newtonian limit contains all 9 independent coefficients in $\bar{s}^{\mu\nu}$, there are only 15 independent combinations of 30 irreducible pieces (out of 60) in $q^{\mu\rho\alpha\nu\beta\sigma\gamma}$ appearing [25]. This is similar for the Lorentz-violating effects on the gravitational-wave propagation in SME, where a subset of 16 of these coefficients appear at leading order [46].

Using the Euler-Lagrange equation,

$$\frac{d}{dt}\frac{\partial L}{\partial \mathbf{v}_a} - \frac{\partial L}{\partial \mathbf{r}_a} = 0,\tag{10}$$

we can obtain from Eq. (7) the acceleration of body a [25],

$$\begin{split} \frac{d^2 r_a^j}{dt^2} &= -\frac{Gm_b}{r^2} \left[\left(1 + \frac{3}{2} \bar{s}_{00} \right) \hat{n}^j - \bar{s}_{jk} \hat{n}^k + \frac{3}{2} \bar{s}_{kl} \hat{n}^k \hat{n}^l \hat{n}^j \right] \\ &+ \frac{2Gm_b}{r^2} \left(\bar{s}_{0j} v^k \hat{n}^k - \bar{s}_{0k} v^k \hat{n}^j \right) \\ &+ \frac{Gm_b}{r^2} \bar{s}_{0k} v_b^l \left[2\delta^{j(k} \hat{n}^{l)} - 3\delta^{kl} \hat{n}^j - 3\hat{n}^j \hat{n}^k \hat{n}^l \right] \\ &+ \frac{Gm_b v^k}{r^3} \left(15\hat{n}^l \hat{n}^m \hat{n}^n \hat{n}_{[j} K_{k]lmn} + 9\hat{n}^l \hat{n}^m K_{[jk]lm} \right. \\ &- 9\hat{n}_{[j} K_{k]llm} \hat{n}^m - 3K_{[jk]ll} \right), \end{split}$$

where $[\cdot]$ denotes the antisymmetrization of indices. The acceleration for body b can be obtained by interchanging the body indices $a \leftrightarrow b$. Again, when $\bar{s}^{\mu\nu} = 0$, the equation reduces to,

$$\frac{d^{2}r_{a}^{j}}{dt^{2}} = -\frac{Gm_{b}}{r^{2}}\hat{n}^{j} + \frac{Gm_{b}v^{k}}{r^{3}}(15\hat{n}^{l}\hat{n}^{m}\hat{n}^{n}\hat{n}_{[j}K_{k]lmn} + 9\hat{n}^{l}\hat{n}^{m}K_{[jk]lm} - 9\hat{n}_{[j}K_{k]llm}\hat{n}^{m} - 3K_{[jk]ll}).$$
(12)

The second term $\propto v/r^3$ of the above equation provides us with a nonstatic (namely velocity-dependent) inverse cubic force between two masses. The behaviour of this term is vastly different from what occurs in GR and other Lorentz-violating terms that preserve the *CPT* symmetry [22,42]. There is no self-acceleration term in (12), which is consistent with the fact that SME is based on an action principle with energy and momentum conservation [21].

Now we discuss the secular changes for a bound orbit with the accleration (12). For an elliptical binary orbit, we use the notations in Damour and Taylor [52]. In particular, the coordinate systems $(\hat{\mathbf{l}}, \hat{\mathbf{J}}, \hat{\mathbf{K}})$ and $(\hat{\mathbf{a}}, \hat{\mathbf{b}}, \hat{\mathbf{c}})$ are defined in Fig. 1. Notations are the same as that in Refs. [35,36], but differ from Refs. [15,25] where $(\vec{P}, \vec{Q}, \vec{k}) \equiv (\hat{\mathbf{a}}, \hat{\mathbf{b}}, \hat{\mathbf{c}})$ was used. To connect the spatial frame $(\hat{\mathbf{a}}, \hat{\mathbf{b}}, \hat{\mathbf{c}})$ with the cannonical Sun-centered celestial-equatorial frame, $(\hat{\mathbf{X}}, \hat{\mathbf{Y}}, \hat{\mathbf{Z}})$, one needs a spatial rotation, \mathcal{R} , to align the axes.

$$\begin{pmatrix} \hat{\mathbf{a}} \\ \hat{\mathbf{b}} \\ \hat{\mathbf{c}} \end{pmatrix} = \mathcal{R} \begin{pmatrix} \hat{\mathbf{X}} \\ \hat{\mathbf{Y}} \\ \hat{\mathbf{Z}} \end{pmatrix}. \tag{13}$$

With the help of $(\hat{\mathbf{I}}, \hat{\mathbf{J}}, \hat{\mathbf{K}})$ in Fig. 1, one can decompose the full rotation into five simple parts, characterized by parameters in celestial mechanics [15,35,36],

$$\mathcal{R} = \mathcal{R}^{(\omega)} \mathcal{R}^{(i)} \mathcal{R}^{(\Omega)} \mathcal{R}^{(\delta)} \mathcal{R}^{(\alpha)}, \tag{14}$$

¹We neglect the boost between these two frames, which is small, with $v/c \approx \mathcal{O}(10^{-3})$, where v is the systematic velocity of the binary pulsar with respect to the Solar System [15,36].

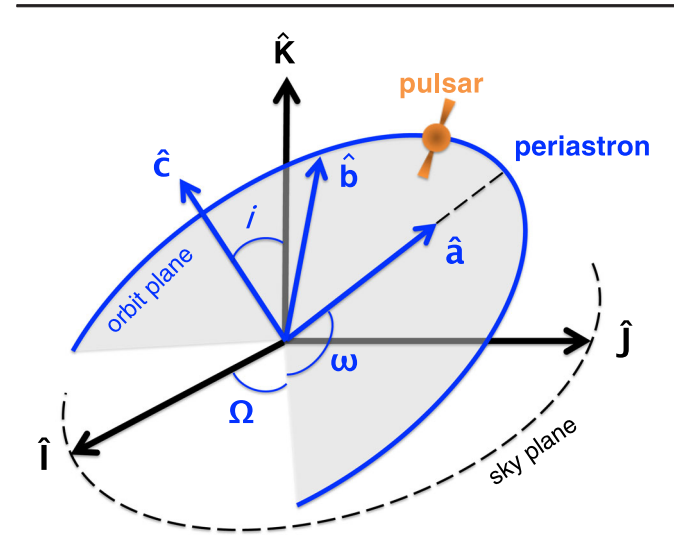


FIG. 1. An illustration of coordinate systems [36]. The frame $(\hat{\mathbf{I}},\hat{\mathbf{J}},\hat{\mathbf{K}})$ is comoving with the pulsar system, with $\hat{\mathbf{K}}$ pointing along the line of sight to the pulsar from the Earth, while $(\hat{\mathbf{I}},\hat{\mathbf{J}})$ constitutes the sky plane with $\hat{\mathbf{I}}$ to east and $\hat{\mathbf{J}}$ to north. The spatial frame $(\hat{\mathbf{a}},\hat{\mathbf{b}},\hat{\mathbf{c}})$ is centered at the pulsar system with $\hat{\mathbf{a}}$ pointing from the center of mass to the periastron, $\hat{\mathbf{c}}$ along the orbital angular momentum, and $\hat{\mathbf{b}} \equiv \hat{\mathbf{c}} \times \hat{\mathbf{a}}$. The frames, $(\hat{\mathbf{I}},\hat{\mathbf{J}},\hat{\mathbf{K}})$ and $(\hat{\mathbf{a}},\hat{\mathbf{b}},\hat{\mathbf{c}})$, are related through rotation matrices, $\mathcal{R}^{(\Omega)}$, $\mathcal{R}^{(i)}$, and $\mathcal{R}^{(\omega)}$.

where

$$\mathcal{R}^{(\alpha)} = \begin{pmatrix} -\sin\alpha & \cos\alpha & 0\\ -\cos\alpha & -\sin\alpha & 0\\ 0 & 0 & 1 \end{pmatrix}, \tag{15}$$

$$\mathcal{R}^{(\delta)} = \begin{pmatrix} 1 & 0 & 0 \\ 0 & \sin \delta & \cos \delta \\ 0 & -\cos \delta & \sin \delta \end{pmatrix}, \tag{16}$$

$$\mathcal{R}^{(\Omega)} = \begin{pmatrix} \cos \Omega & \sin \Omega & 0 \\ -\sin \Omega & \cos \Omega & 0 \\ 0 & 0 & 1 \end{pmatrix}, \tag{17}$$

$$\mathcal{R}^{(i)} = \begin{pmatrix} 1 & 0 & 0 \\ 0 & \cos i & \sin i \\ 0 & -\sin i & \cos i \end{pmatrix}, \tag{18}$$

$$\mathcal{R}^{(\omega)} = \begin{pmatrix} \cos \omega & \sin \omega & 0 \\ -\sin \omega & \cos \omega & 0 \\ 0 & 0 & 1 \end{pmatrix}. \tag{19}$$

In the rotation matrix, α and δ are the right ascension and declination of the binary pulsar, i is the orbital inclination, ω is the longitude of the periastron, and Ω is the longitude of the ascending node (see Fig. 1).

Using the techniques of osculating elements, Bailey and Havert [25] obtained the secular changes of orbital elements after averaging over the orbital-period timescale,

$$\left\langle \frac{da}{dt} \right\rangle = 0,$$
 (20)

$$\left\langle \frac{de}{dt} \right\rangle = 0,$$
 (21)

$$\left\langle \frac{d\omega}{dt} \right\rangle = -\frac{n_b^2}{4(1-e^2)^{3/2}} \left\{ 2K_1 + \cot i \left[K_2 \cos \omega + K_3 \sin \omega \right] \right\},$$
(22)

$$\left\langle \frac{di}{dt} \right\rangle = \frac{n_b^2}{4(1 - e^2)^{3/2}} [K_3 \cos \omega - K_2 \sin \omega], \quad (23)$$

$$\left\langle \frac{d\Omega}{dt} \right\rangle = \frac{n_b^2}{4(1 - e^2)^{3/2}} \csc i[K_2 \cos \omega + K_3 \sin \omega], \qquad (24)$$

where a is the semimajor axis, e is the orbital eccentricity, and $n_b \equiv 2\pi/P_b$ with P_b the orbital period. In above equations, K_1 , K_2 , K_3 are defined by [25],

$$K_1 \equiv 3K_{\hat{a}\,\hat{a}\,\hat{a}\,\hat{b}} + K_{\hat{a}\,\hat{b}\,\hat{b}\,\hat{b}} + 6K_{[\hat{a}\,\hat{b}]\hat{c}\,\hat{c}},\tag{25}$$

$$K_2 \equiv 3K_{\hat{a}\hat{b}\hat{b}\hat{c}} - 3K_{\hat{a}\hat{a}\hat{a}\hat{c}} - 4K_{\hat{a}\hat{c}\hat{c}\hat{c}} - 6K_{\hat{b}\hat{a}\hat{b}\hat{c}}, \quad (26)$$

$$K_3 \equiv 6K_{\hat{a}\,\hat{a}\,\hat{b}\,\hat{c}} + 4K_{\hat{b}\,\hat{c}\,\hat{c}\,\hat{c}} - 3K_{\hat{b}\,\hat{a}\,\hat{a}\,\hat{c}} + 3K_{\hat{b}\,\hat{b}\,\hat{b}\,\hat{c}}, \quad (27)$$

where the indices on the right-hand sides denote the projection of K_{jklm} in Eq. (9) onto the $(\hat{\mathbf{a}}, \hat{\mathbf{b}}, \hat{\mathbf{c}})$ directions. More details can be found in Ref. [25].

III. BINARY PULSARS

Our starting point to put constraints on the SME coefficients with binary pulsars will be using the secular changes in orbital elements. In general, pulsar timing is insensitive to the longitude of the ascending node Ω , unless the binary is very nearby [53,54]. Thus, the secular changes in the orbital inclination and the longitude of the periastron are the most relevant to our tests. A nonzero $\langle di/dt \rangle$ will be reflected in the accurately measured, projected semimajor axis of the pulsar orbit, $x_p \equiv a_p \sin i/c$, where $a_p \simeq m_2 a/(m_1 + m_2)$ is the semimajor axis of the pulsar orbit. From Eq. (23), one has,

 $^{^{2}}$ We hereafter use m_{1} and m_{2} to denote the masses of the pulsar and its companion, respectively.

	PSR B1913 + 16	PSR B1534 + 12	PSR B2127 + 11C	PSR J0737 – 3039A
Observational span, $T_{\rm obs}$ (year)	~31	~22	~12	~2.7
Right ascension, α (J2000)	19h15m27s99942(3)	15h37m09s961730(3)	21h30m01s2042(1)	07h37m51s24927(3)
Declination, δ (J2000)	16°06′27″3868(5)	11°55′55″43387(6)	12°10′38″209(4)	-30°39′40″7195(5)
Orbital period, P_b (day)	0.322997448918(3)	0.420737298879(2)	0.33528204828(5)	0.10225156248(5)
Eccentricity, e	0.6171340(4)	0.27367752(7)	0.681395(2)	0.0877775(9)
Pulsar's projected semimajor axis, x_p (lt-s)	2.341776(2)	3.7294636(6)	2.51845(6)	1.415032(1)
Longitude of periastron, ω (deg)	292.54450(8)	283.306012(12)	345.3069(5)	87.0331(8)
Epoch of periastron, T_0 (MJD)	52144.90097849(3)	52076.827113263(11)	50000.0643452(3)	53155.9074280(2)
Advance of periastron, $\dot{\omega}$ (deg yr ⁻¹)	4.226585(4)	1.7557950(19)	4.4644(1)	16.89947(68)
Time derivative of x_p , \dot{x}_p	$-1.4(9) \times 10^{-14}$	$ \dot{x}_p < 3.0 \times 10^{-15} *$	$ \dot{x}_p < 5.5 \times 10^{-13} *$	$ \dot{x}_p < 4.1 \times 10^{-14} *$
Parameters used to derive masses	$\gamma \& \dot{P}_b$	γ & s	$\gamma \& \dot{P}_b$	R & s
Pulsar mass, m_1 (M_{\odot})	1.435(2)	1.364(20)	1.36(4)	1.339(3)
Companion mass, m_2 (M_{\odot})	1.390(1)	1.356(7)	1.36(2)	1.250(2)
Excess of $\dot{\omega}$, $\dot{\omega} - \dot{\omega}^{GR}$ (deg yr ⁻¹)	0.003(3)	-0.018(12)	0.00(6)	-0.01(2)

TABLE I. Relevant timing parameters for PSRs B1913 + 16 [55], B1534 + 12 [56], B2127 + 11C [48], and J0737 - 3039A [57]. Parenthesized numbers represent the 1- σ uncertainty in the last digits quoted. Estimated parameters are marked with "*".

$$\left\langle \frac{\dot{x}_p}{x_p} \right\rangle = \frac{n_b^2 \cot i}{4(1 - e^2)^{3/2}} [K_3 \cos \omega - K_2 \sin \omega]. \quad (28)$$

In the following, we will make use of Eqs. (22) and (28), naming them as the $\dot{\omega}$ -test and the \dot{x}_p -test respectively, to put bounds on the coefficients for Lorentz/CPT violation. It is apparent from Eqs. (22) and (28) that binary pulsars with small orbits will provide tight constraints. Besides the smallness of the orbit, there are other criteria to meet for binary pulsars, that will become clear later. According to the needs for the $\dot{\omega}$ -test and/or the \dot{x}_p -test, we carefully pick 11 well-timed binary pulsars with relativistic orbits. We categorize them into three groups:

- (1) Group I: relativistic double NS binaries with orbital period smaller than 1 day. We pick 4 binary pulsars: PSRs B1913 + 16 [55], B1534 + 12 [56], B2127 + 11C [48], and J0737 3039A [57]. Relevant timing parameters for our tests are listed in Table I.
- (2) Group II: relativistic neutron-star—white-dwarf (NS-WD) binaries with orbital period smaller than 1 day, and whose WD companions were well studied with optical observations. We pick 3 binary pulsars: PSRs J0348 + 0432 [58], J1738 + 0333 [59], and J1012 + 5307 [60]. Relevant timing parameters for our tests are listed in Table II.
- (3) Group III: relativistic NS-WD binaries with orbital period smaller than 2 days, and whose Shapiro delays were also identified in the timing observations. We pick 4 binary pulsars: PSRs J0751 + 1807 [61], J1802 2124 [62], J1909 3744 [61], and J2043 + 1711 [63]. Relevant timing parameters for our tests are listed in Table III.

These 11 binary pulsars all have been monitored for years, most of which were regularly observed within the pulsar-timing-array projects, including the Parks Pulsar Timing Array (PPTA) [66], the European Pulsar Timing

Array (EPTA) [67], and the North American Nanohertz Observatory for Gravitational Waves (NANOGrav) [68]. To successfully achieve the proposed $\dot{\omega}$ -test and/or \dot{x}_p -test, we address the following concerns:

- (i) Because \dot{x}_p was not always fitted for in deriving the timing solution of binary pulsars, wherever it is inaccessible, we conservatively estimate a 1- σ upper limit from the uncertainty of x_p , as $|\dot{x}_p|^{\text{upper}} =$ $\sqrt{12}\sigma_{x_n}/T_{\rm obs}$ [35], where $T_{\rm obs}$ is the time span used in deriving the timing solution. The prefactor " $\sqrt{12}$ " was inspired by a linear-in-time evolution. Actually as was already noticed for PSR B1534 + 12, this is a quite good estimation [35]. In addition, PSR B1913 + 16 was estimated by Shao [35] to have $|\dot{x}_p|^{\text{upper}} = 1.3 \times 10^{-14}$ using the results of Weisberg et al. [69] where \dot{x}_p was not reported. Recently, Weisberg and Huang [55] fitted for \dot{x}_p , and obtained $\dot{x}_p = (-1.4 \pm 0.9) \times 10^{-14}$ in excellent agreement with the estimation. This further gives us confidence in using the estimation formula. Estimated \dot{x}_n 's are decorated with "*" in Tables I-III.
- (ii) Sometimes for nearby binary pulsars, there is a contribution to \dot{x}_p from the proper motion of the binary [53],

$$\left(\frac{\dot{x}_p}{x_p}\right)^{\text{PM}} = \left(-\mu_\alpha \sin \Omega + \mu_\delta \cos \Omega\right) \cot i, \quad (29)$$

where μ_{α} and μ_{δ} are proper motions in α and δ directions respectively [54]. It could produce a nonzero \dot{x}_p , as was measured for several binary pulsars. Assuming GR as the theory of gravity, this piece of information can be used to constrain Ω . Here we do not assume GR and stay agnostic about the longitude of ascending node. We randomly

TABLE II. Relevant timing parameters for PSRs J0348 + 0432 [58], J1738 + 0333 [59], and J1012 + 5307 [60]. Parenthesized numbers represent the 1- σ uncertainty in the last digits quoted. The listed Laplace-Lagrange parameter, η , is the intrinsic value, after subtraction of the contribution from the Shapiro delay [64]. Masses are derived from the combination of optical and radio observations, and they are independent of the underlying gravity theory [21,65]. Estimated parameters are marked with "*".

	PSR J0348 + 0432	PSR J1738 + 0333	PSR J1012 + 5307
Observational span, T_{obs} (year)	~3.7	~10.0	~15.0
Right ascension, α (J2000)	$03^{h}48^{m}43^{s}639000(4)$	17h38m53s9658386(7)	10 ^h 12 ^m 33 ^s 4341010(99)
Declination, δ (J2000)	04°32′11″4580(2)	03°33′10″86667(3)	53°07′02″60070(13)
Orbital period, P_b (day)	0.102424062722(7)	0.3547907398724(13)	0.60467271355(3)
Pulsar's projected semimajor axis, x_p (lt-s)	0.14097938(7)	0.343429130(17)	0.5818172(2)
$\eta \equiv e \sin \omega$	$(1.9 \pm 1.0) \times 10^{-6}$	$(-1.4 \pm 1.1) \times 10^{-7}$	$(-1.4 \pm 3.4) \times 10^{-7}$
$\kappa \equiv e \cos \omega$	$(1.4 \pm 1.0) \times 10^{-6}$	$(3.1 \pm 1.1) \times 10^{-7}$	$(0.6 \pm 3.1) \times 10^{-7}$
Time derivative of x_p , \dot{x}_p	$ \dot{x}_p < 2.1 \times 10^{-15} *$	$(0.7 \pm 0.5) \times 10^{-15}$	$(2.3 \pm 0.8) \times 10^{-15}$
Pulsar mass, m_1 (M_{\odot})	2.01(4)	$1.46^{+0.06}_{-0.05}$	1.64(22)
Companion mass, m_2 (M_{\odot})	0.172(3)	$0.181^{+0.008}_{-0.007}$	0.16(2)

TABLE III. Relevant timing parameters for PSRs J0751 + 1807 [61], J1802 – 2124 [62], J1909 – 3744 [61], and J2043 + 1711 [63]. Parenthesized numbers represent the 1- σ uncertainty in the last digits quoted. Estimated parameters are marked with "*".

	PSR J0751 + 1807	PSR J1802 – 2124	PSR J1909 – 3744	PSR J2043 + 1711
Observational span, $T_{\rm obs}$ (year)	~17.6	~6.4	~9.4	~4.5
Right ascension, α (J2000)	07h51m09s155331(13			20 ^h 43 ^m 20 ^s 881730(1)
Declination, δ (J2000)	18°07′38″4864(10)	-21°24′03″649(2)	-37°44′14″51561(3)	17°11′28″91265(3)
Orbital period, P_b (day)	0.263144270792(7)	0.698889243381(5)	1.533449474329(13)	1.482290786394(15)
Pulsar's projected semimajor axis, x_p (lt-s	0.3966158(3)	3.7188533(5)	1.89799099(6)	1.62395834(15)
$\eta \equiv e \sin \omega$	$(3.3 \pm 0.5) \times 10^{-6}$	$(8.6 \pm 0.9) \times 10^{-7}$	$(0 \pm 1.9) \times 10^{-8}$	$(-4.07 \pm 0.07) \times 10^{-6}$
$\kappa \equiv e \cos \omega$	$(3.8 \pm 5.0) \times 10^{-7}$	$(2.32 \pm 0.04) \times 10^{-6}$	$(-1.22 \pm 0.11) \times 10^{-7}$	$7(-2.67 \pm 0.05) \times 10^{-6}$
Time derivative of x_p , \dot{x}_p	$(-4.9 \pm 0.9) \times 10^{-15}$	$ \dot{x}_p < 8.5 \times 10^{-15} *$	$(0.6 \pm 1.7) \times 10^{-16}$	$ \dot{x}_p < 3.7 \times 10^{-15} *$
Parameters used to derive masses	$\dot{P}_b \& \zeta$	r & s	r & s	$h_3 \& \zeta$
Pulsar mass, m_1 (M_{\odot})	1.64(15)	1.24(11)	1.540(27)	$1.38^{+0.12}_{-0.13}$
Companion mass, m_2 (M_{\odot})	0.16(1)	0.78(4)	0.2130(24)	0.173(10)

- distribute it uniformly in the range $\Omega \in [0, 360^{\circ})$; thus the net effect from Eq. (29) after averaging over Ω vanishes. For these pulsars with reported \dot{x}_p 's, we take the uncertainty of the observed \dot{x}_p as an estimate for its upper limit.
- (iii) Usually, for double NS binaries in Group I, the total mass of the binary is calculated from the very well measured $\dot{\omega}$ [54]. For consistency, the $\dot{\omega}$ -test is invalid if masses were derived from the observed $\dot{\omega}$ by assuming GR. Therefore, we need to recalculate masses without using the measured $\dot{\omega}$. We performed such calculations for PSRs B1913 + 16, B1534 + 12, B2127 + 11C, and J0737 – 3039A. Results are listed in Table I. By using these $\dot{\omega}$ -independent masses, we recalculate the periastron advance rate with GR, and obtain the excess of $\dot{\omega}$ by substracting it from the observed value. By doing so, we obtain a "clean" $\dot{\omega}$ -test. The uncertainties in the excess of $\dot{\omega}$ are dominated by the uncertainties of the masses, and as a cost the clean $\dot{\omega}$ -test usually gives much worse limits than those
- from \dot{x}_p (see Table IV). This will be the bottleneck for our global analysis (see below).
- (iv) One caution in directly using the secular change of ω in Lorentz-violating theories was pointed out by Wex and Kramer [70], that a large $\dot{\omega}$ can render the secular changes nonconstant. These effects cannot be too large based on the fact that all binaries were well fitted with simple timing models. In our samples, the biggest change in ω is ~100° for PSR B1913 + 16 [55]. Therefore, we consider it safe to use time-averaged values for ω -related quantities as a rough approximation at current stage.³ For example, in Eqs. (22) and (28), we use the ω value in the middle of the observational span. In principle, a timing model with nonlinear-intime evolution of ω would be perfect in addressing this issue [70], which is rather complicated and it is

³This will not be valid for the (unpublished) new timing solution of the double pulsar [57,71] where, assuming GR, up to now a change in ω is > 250° already.

Pulsar	Test	$1 - \sigma$ constraint
PSR J0348 + 0432	\dot{x}_p	$ 0.81K_2 - 0.59K_3 < 30 \text{ m}$
PSR J0737 – 3039A	$\dot{x}_p^{'}$	$ 0.99K_2 - 0.13K_3 < 2.0 \text{ km}$
	$\dot{\hat{\omega}}$	$ 2K_1 + 0.03K_3 < 26 \text{ km}$
PSR J0751 + 1807	\dot{x}_p	$ 0.99K_2 - 0.11K_3 < 81 \text{ m}$
PSR J1012 + 5307	\dot{x}_p	$ 0.92K_2 + 0.39K_3 < 140 \text{ m}$
PSR B1534 + 12	$egin{array}{c} \dot{x}_p \ \dot{x}_p \ \dot{x}_p \ \dot{\omega} \end{array}$	$ 0.97K_2 + 0.24K_3 < 132 \text{ m}$
	$\dot{\hat{m{\omega}}}$	$ 2K_1 + 0.05K_2 - 0.21K_3 < 240 \text{ km}$
PSR J1738 + 0333	$\dot{x}_p \ \dot{x}_p$	$ 0.41K_2 + 0.91K_3 < 27 \text{ m}$
PSR J1802 – 2124	\dot{x}_p	$ 0.35K_2 - 0.94K_3 < 1.8 \text{ km}$
PSR J1909 – 3744	\dot{x}_{p}	$ K_3 < 670 \text{ m}$
PSR B1913 + 16	$\dot{\hat{x_p}}$ $\dot{x_p}$	$ 0.99K_2 - 0.16K_3 < 48 \text{ m}$
	$\dot{\hat{m{\omega}}}$	$ 2K_1 - 0.15K_2 - 0.92K_3 < 19 \text{ km}$
PSR J2043 + 1711	\dot{x}_p	$ 0.84K_2 - 0.55K_3 < 8.6 \text{ km}$
PSR B2127 + 11C	\dot{x}_p	$ 0.29K_2 + 0.96K_3 < 2.6 \text{ km}$
	$\dot{\dot{\omega}}$	$ 2K_1 + 0.80K_2 - 0.25K_3 < 330 \text{ km}$

TABLE IV. Constraints on K_i (i = 1, 2, 3) from binary pulsars. Notice that the definition of K_i depends on the geometry of the binary through projections in Eqs. (25)–(27).

beyond the scope of this work (see Ref. [70] for a simplified version when assuming an edge-on orbit, approximating the double pulsar).

- (v) As was pointed out several times, Ω is in general not determined in pulsar timing. We will treat it a random variable uniformly distributed in $\Omega \in [0, 360^{\circ})$. This choice makes our tests "probabilistic tests."
- (vi) To perform the $\dot{\omega}$ -test and the \dot{x}_p -test, component masses of the binary are needed sometimes. We have discussed the situation for double NS binaries in Group I. For NS-WD binaries in Group II, we use the masses derived from the optical observation of the WD. These masses are independent of the gravity theories [21,65] (see Table II). For NS-WD binaries in Group III, we derive masses from the measurement of the Shapiro delay for PSRs J1802 2124, J1909 3744, and J2043 + 1711, while for PSR J0751 + 1807, we also used the

orbital decay measurement for assistance (see Table III). These calculation assumes that the deviations from GR are small, in consistent with the observational results, as well as the effective-field-theory framework. Nevertheless, we might overlook strong-field effects that arise in some specific theories [44,45,72] (see Sec. IV).

Taking the above considerations into account, we have derived a set of independent limits on various linear combinations of coefficients for Lorentz/CPT violation, making use of $4\dot{\omega}$ -tests and $11\dot{x}_p$ -tests from the pulsars in Tables I–III. These results are tabulated in Table IV, and the best ones are in agreement with the estimation by Bailey and Havert [25]. Notice that, the results in Table IV should be directly compared with the *estimated sensitivity* in the Table I of Ref. [25]. The estimated sensitivities for other experiments, namely the Solar system ephemeris, laser ranging, gravimeter, short-range gravity, and time delay, are expected to be orders of magnitude weaker. Nevertheless, it

TABLE V. Limits on different components of $q^{\mu\rho\alpha\nu\beta\sigma\gamma}$, assuming only one of them is nonzero. Components $q^{XYZXYZT}$ and $q^{XYZXZYT}$ do not enter the tests from binary pulsars, thus they remain unconstrained.

Coefficient	1- <i>σ</i> limit [m]	Coefficient	$1-\sigma$ limit [m]	Coefficient	$1-\sigma$ limit [m]
q^{TXYTXTX}	22	q^{TXYTXTY}	11	q^{TXYTXTZ}	12
q^{TXYTYTY}	10	q^{TXYTYTZ}	5.7	q^{TXYTZTZ}	9.7
q^{TXYXYXY}	8.0	q^{TXYXYXZ}	8.3	q^{TXYXYYZ}	6.2
q^{TXYXZXZ}	8.3	q^{TXYXZYZ}	3.7	q^{TXYYZYZ}	5.3
q^{TXZTXTX}	24	q^{TXZTXTY}	10	q^{TXZTXTZ}	11
q^{TXZTYTY}	6.2	q^{TXZTYTZ}	4.8	q^{TXZTZTZ}	18
q^{TXZXZXZ}	27	q^{TXZXZYZ}	11	q^{TXZYZYZ}	6.5
q^{TYZYZYZ}	8.8	$q^{XYZXYXT}$	29	$q^{XYZXYYT}$	14
$q^{XYZXYZT}$		$q^{XYZXZXT}$	13	$q^{XYZXZYT}$	
$q^{XYZXZZT}$	14	$q^{XYZYZYT}$	13	$q^{XYZYZZT}$	29

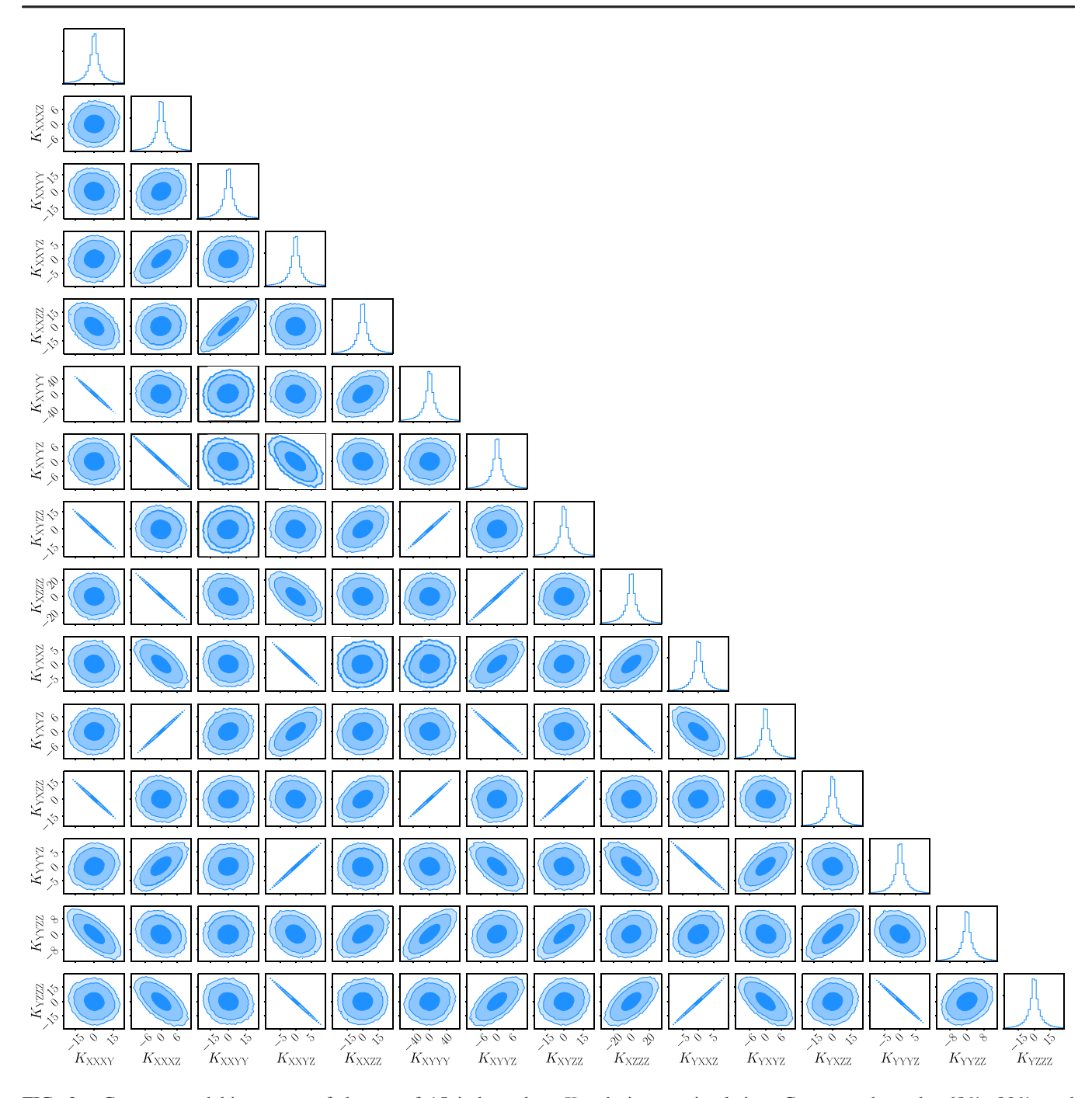


FIG. 2. Contours and histograms of the set of 15 independent K_{jklm} 's in our simulation. Contours show the 68%, 90%, and 95% confidence levels. The unit for K_{jklm} is 10^6 m in this figure.

would still be valuable to work out the actual limits that these experiments would cast; they might probe some components of $q^{\mu\rho\alpha\nu\beta\sigma\gamma}$ which binary pulsars are insensitive to study (see below).

The limits in Table IV are not of fundamental value. K_i 's (i=1,2,3) are system dependent through the projections defined in Eqs. (25)–(27), where projections are given explicitly in Eqs. (13)–(19) with various angles different for individual pulsars. This is the power of many pulsar systems that are in principle able to break any parameter

degeneracy [35,36]. In order to convert the limits in Table IV into limits on the underlying Lorentz-violating coefficients $q^{\mu\rho\alpha\nu\beta\sigma\gamma}$ in the Lagrangian (5), we use Eq. (9) to relate K_{iilm} with $q^{\mu\rho\alpha\nu\beta\sigma\gamma}$.

The limits in Table IV are limits on different linear combinations of $q^{\mu\rho\alpha\nu\beta\sigma\gamma}$. For a $1-\sigma$ limit "a," we denote it as $|\mathcal{X}_a(q^{\mu\rho\alpha\nu\beta\sigma\gamma},\Omega_a)|<\mathcal{C}_a$ where the longitude of the ascending node Ω_a is unknown in general. To proceed practically, we adopt the probabilistic density function,

Symbol Definition $1-\sigma$ limit [10^6 m] $\frac{1}{2}(-q^{\text{TXYTXTX}} + q^{\text{TXYXYXY}} + q^{\text{TXYXZXZ}} - q^{\text{XYZXZXT}})$ K_{XXXY} 6.6 $\frac{1}{2}(q^{\text{TXYXYXZ}} - q^{\text{TXZTXTX}} + q^{\text{TXZXZXZ}} + q^{\text{XYZXYXT}})$ K_{XXXZ} 3.1 $\frac{1}{2}(-2q^{\text{TXYTXTY}} + 2q^{\text{TXYXZYZ}} + q^{\text{XYZXYZT}} - 2q^{\text{XYZXZYT}})$ K_{XXYY} 7.1 $\frac{3}{2}(-2q^{\text{TXYTXTZ}} - 2q^{\text{TXYXYYZ}} - 2q^{\text{TXZTXTY}} + 2q^{\text{TXZXZYZ}} + q^{\text{XYZXYYT}} - q^{\text{XYZXZZT}})$ $K_{\rm XXYZ}$ 2.7 $\frac{1}{3}(-2q^{\text{TXYXZYZ}} - 2q^{\text{TXZTXTZ}} + 2q^{\text{XYZXYZT}} - q^{\text{XYZXZYT}})$ $K_{\rm XXZZ}$ 8.1 $-q^{\text{TXYTYTY}} + q^{\text{TXYXYXY}} + q^{\text{TXYYZYZ}} - q^{\text{XYZYZYT}}$ K_{XYYY} 20 $\frac{1}{2}(-2q^{\text{TXYTYTZ}} + 3q^{\text{TXYXYXZ}} - q^{\text{TXZTYTY}} + q^{\text{TXZYZYZ}} - q^{\text{XYZYZZT}})$ K_{XYYZ} 3.1 $\frac{1}{2}(-q^{\text{TXYTZTZ}} + 3q^{\text{TXYXZXZ}} + q^{\text{TXYYZYZ}} - 2q^{\text{TXZTYTZ}} - q^{\text{XYZYZYT}})$ K_{XYZZ} 6.6 $-q^{\text{TXZTZTZ}} + q^{\text{TXZXZXZX}} + q^{\text{TXZYZYZ}} - q^{\text{XYZYZZT}}$ K_{XZZZ} 9.3 $\frac{1}{2}(3q^{\text{TXYTXTZ}} + 3q^{\text{TXYXYYZ}} - q^{\text{TXZTXTY}} + q^{\text{TXZXZYZ}} + q^{\text{XYZXZZT}})$ $K_{\rm YXXZ}$ 2.7 $\frac{1}{6}(4q^{\text{TXYTYTZ}} - 2q^{\text{TXYXYXZ}} - 2q^{\text{TXZTYTY}} + 2q^{\text{TXZYZYZ}} + q^{\text{XYZXYXT}} + q^{\text{XYZYZZT}})$ $K_{\rm YXYZ}$ 3.1 $\frac{1}{3}(3q^{\text{TXYTZTZ}} - q^{\text{TXYXZXZ}} - 3q^{\text{TXYYZYZ}} - 2q^{\text{TXZTYTZ}} + q^{\text{XYZXZXT}})$ $K_{\rm YXZZ}$ 6.6 $\frac{1}{3}(q^{\text{TXYXYYZ}} - q^{\text{TXZTYTY}} + q^{\text{TYZYZYZ}} + q^{\text{XYZXYYT}})$ $K_{\rm YYYZ}$ 2.7 $\frac{1}{2}(2q^{\text{TXYXZYZ}} - 2q^{\text{TXZTYTZ}} + q^{\text{XYZXYZT}} + q^{\text{XYZXZYT}})$ K_{YYZZ} 4.0 $-q^{\text{TXZTZTZ}} + q^{\text{TXZXZYZ}} + q^{\text{TYZYZYZ}} + q^{\text{XYZXZZTZ}}$ 8.0 K_{YZZZ}

TABLE VI. Global constraints on the canonical set of 15 K_{iklm} .

$$P(q^{\mu\rho\alpha\nu\beta\sigma\gamma}) \propto \prod_{a} \int_{0}^{2\pi} \frac{1}{\sqrt{2\pi}} \exp\left\{-\frac{1}{2} \left| \frac{\mathcal{X}_{a}(q^{\mu\rho\alpha\nu\beta\sigma\gamma}, \Omega_{a})}{\mathcal{C}_{a}} \right|^{2} \right\} \times \frac{d\Omega_{a}}{2\pi}, \tag{30}$$

where we have made assumptions on the Gaussianity of measurements and that the limits on K_i 's in Table IV are mutually independent. In Eq. (30) we have also marginalized over the unknown angles Ω_a , as a *nuisance* parameter in the language of Bayesian statistics [73].

As mentioned in Sec. II, from Young tableaux it was established that there are 60 independent coefficients for $q^{\mu\rho\alpha\nu\beta\sigma\gamma}$, while only a subset of 30 (in the form of 15 independent linear combinations) could appear in our pulsar tests [25]. We identify them explicitly. We find that, actually 2 of these 30 coefficients, $q^{XYZXYZT}$ and $q^{XYZXZYT}$, do not show up. This phenomenon was already met in other contexts of SME [74]. It tells us that binary-pulsar tests will not be able to constrain these 2 components, and even if they are large, they can escape from our tests. They need to be constrained with other experiments. The conclusion is worked out through an explicit calculation, but we do not have a clear physical understanding why this particular set of coefficients are relevant to binary pulsars. However, relaxing the assumptions (i.e., post-Newtonian order $\mathcal{O}(v/c)$ beyond the Newtonian limit) and using spinweighted spherical harmonics could reveal more precisely the underlying reasons for the combinations of coefficients appearing in this analysis [22,75,76]. We hope it stimulates other groups to analyze their experiments, and obtain a better understanding.

As a first attempt to constrain $q^{\mu\rho\alpha\nu\beta\sigma\gamma}$, we treat only one of them as nonzero. The final limit comes from a properly weighted combination of the 15 tests in Table IV. The

results are listed in Table V. In the scenario where only one of $q^{\mu\rho\alpha\nu\beta\sigma\gamma}$ is nonzero, the constraint is derived predominantly from the tightest ones in Table IV. The coefficients for Lorentz/*CPT* violation $q^{\mu\rho\alpha\nu\beta\sigma\gamma}$ are limited to $\mathcal{O}(1-10 \text{ m})$, as predicted by Bailey and Havert [25].

In addition, we perform a global test where all 15 independent combinations of $q^{\mu\rho\alpha\nu\beta\sigma\gamma}$ could be nonzero. In this case, we use a set of 15 canonical K_{iklm} to represent these linear combinations. They are identified explicitly and are given in terms of $q^{\mu\rho\alpha\nu\beta\sigma\gamma}$ in the second column of Table VI. Since we have 15 independent terms, we have to use all 15 tests given in Table IV. As was done for $\bar{s}^{\mu\nu}$ in Ref. [35], Monte Carlo simulations are set up to properly account for the measurements and the unknown Ω 's. Our results are given in Fig. 2, and the marginalized distributions are utilized to derive the 1- σ constraints on the set of 15 canonical K_{jklm} , and they are given in the last column of Table VI. In this scenario we are only able to constrain K_{iklm} to the level $\mathcal{O}(10^6 \text{ m})$. The direct limits in Table IV are quite heteroscedastic, spanning from $\mathcal{O}(10 \text{ m})$ to $\mathcal{O}(10^5 \text{ m})$. Because of this, the global analysis gives limits corresponding more or less to the worst limits in Table IV with strong correlations between some coefficients (see Fig. 2). In the future, more tests will tighten these limits.

Our results in Tables V and VI constitute the first set of systematic limits from pulsar timing experiments on $q^{\mu\rho\alpha\nu\beta\sigma\gamma}$. They are also the first set of constraints from the post-Newtonian dynamics of binaries with *CPT*-violating operators in SME for the gravity sector, complementary to the unique limit obtained from the kinematics in the propagation of gravitational waves [46]. Because the SME is viewed as an *effective field theory*, the coefficients for Lorentz/*CPT* violation are not fixed *a priori* [14,15]. In general, specific theories are needed to cast predictions for

their values. We here undertake an agnostic way, and let data decide the values they can have and the constraints they should satisfy. Our results can be mapped to theory parameters if a theory is specified.

IV. DISCUSSIONS

Searching for new physics beyond the current paradigm is a rewarding task. Up to now, no violation in Lorentz and CPT symmetries has been convincingly found [9,19,21]. When the deviation is perturbatively small, the effectivefield-theory framework of SME provides a practically useful platform to systematically study these tiny deviations. Many new phenomena were discovered in SME for the past decades. Here we specifically study the pure gravity sector of SME in the presence of CPT-violating leading-order operators with mass dimension 5. These operators are interesting in the following manner. While being of higher mass dimension than those of GR and the leading-order Lorentz-violating operators which are of mass dimension 4, they can be better probed with astronomical observations instead of short-range experiments [25]. The insensitivity of short-range laboratory experiments is due to the nature of CPT violation where, an additional suppression factor, proportional to $(v_a - v_b)/c$, is present. In order to confine short-range experiments within laboratories for a long duration for precision measurement, this factor appears enormously small. In contrast, for relativistic binary pulsars with $P_h \lesssim 1$ day, this factor can be as large as 10^{-3} . Therefore, binary pulsars become even more powerful than short-range experiments to constrain these operators.

Motivated by this observation, in this paper we have utilized binary pulsars to constrain these operators, using the analytical post-Newtonian results for a binary orbit from Bailey and Havert [25]. By taking care of all caveats from observational facts, we tailored the results into a form that can immediately be used in analysing binary pulsars. Well-timed relativistic binary pulsars turn out to be suitable for the tests, and we put constraints on the coefficients for Lorentz/CPT violation to $\mathcal{O}(10 \text{ m})$ when only one coefficient is allowed to be nonzero (see Table V), and to $\mathcal{O}(10^6 \text{ m})$ when all coefficients can be nonzero at the same time (see Table VI). They represent the first set of observational constraints for CPT-violating gravity in SME from the post-Newtonian dynamics, complementing the kinematic constraints from gravitational waves [46].

Since the SME is based on the perturbative nature of effective field theories [14] and in particular here we have used the linearized gravity [17,25], our limits on $q^{\mu\rho\alpha\nu\beta\sigma\gamma}$

cannot probe nonperturbative effects that might arise with the strong gravitational fields of NSs, like the "scalarization" phenomenon in scalar-tensor theories [44,45,59,72]. Strictly speaking, our limits are effective limits for the strong-field counterparts of $q^{\mu\rho\alpha\nu\beta\sigma\gamma}$. Nevertheless, usually the strong-field limits are more restricting than their weak-field counterparts. Thus, our results are actually conservative in this respect. The constancy of $q^{\mu\rho\alpha\nu\beta\sigma\gamma}$ in our work is an assumption that is required for the energy-momentum conservation of the Lagrangian [14]. It does not leave out the possibility of variations in these coefficients on timescales longer than those in which the Sun-centered frame is approximately inertial, i.e., a few hundreds of years. In more general cases, e.g., when considering the strong-field effects from NSs. one might get body-dependent, or in some cases even position-dependent coefficients for Lorentz/CPT violation (e.g., a term similar to the Whitehead's term in the parametrized post-Newtonian framework [77-80]). But this will need some specific theoretic inputs and is beyond the scope of this work.

Pulsar timing in the future will further improve the measurements of binary orbits, and provide better limits on possible new physics. In our case, the measurement precisions for $\dot{\omega}$ and \dot{x}_p both improve as $T^{-3/2}$ [52] where T is the observational time span, even without improvements in the telescopes. Nevertheless, we in addition have new telescopes and technologies coming online. The upcoming observations at the Five-hundred-meter Aperture Spherical Telescope (FAST) [81] and the Square Kilometre Array (SKA) [82,83] are guaranteed to boost the timing precision. Also, they will discover more binary pulsars to perform the tests. Therefore, the actual improvement in constraining the coefficients for Lorentz/ CPT violation will be significantly faster than $T^{-3/2}$.

ACKNOWLEDGMENTS

We thank Alan Kostelecký and Norbert Wex for helpful discussions, and Paulo Freire for carefully reading the manuscript. We also thank the anonymous referee for helpful comments. This work was supported by the National Science Foundation of China (11721303), and XDB23010200. L. S. acknowledges financial support by the European Research Council (ERC) for the ERC Synergy Grant BlackHoleCam under Contract No. 610058, and is grateful to the Mainz Institute for Theoretical Physics (MITP) for its hospitality and its partial support during the completion of this work.

- [1] H. F. M. Goenner, Living Rev. Relativity 7, 2 (2004).
- [2] S. Liberati, Classical Quantum Gravity 30, 133001 (2013).
- [3] J. D. Tasson, Rep. Prog. Phys. 77, 062901 (2014).
- [4] C. M. Will, arXiv:1409.7871.
- [5] V. A. Kostelecký and S. Samuel, Phys. Rev. D 39, 683 (1989).
- [6] C. P. Burgess, Living Rev. Relativity 7, 5 (2004).
- [7] S. Hossenfelder, Living Rev. Relativity 16, 2 (2013).
- [8] T. Clifton, P. G. Ferreira, A. Padilla, and C. Skordis, Phys. Rep. 513, 1 (2012).
- [9] C. M. Will, Living Rev. Relativity 17, 4 (2014).
- [10] J. D. Tasson, Symmetry 8, 111 (2016).
- [11] S. Weinberg, Proc. Sci., CD09 (2009) 001.
- [12] D. Colladay and V. A. Kostelecký, Phys. Rev. D 55, 6760 (1997).
- [13] D. Colladay and V. A. Kostelecký, Phys. Rev. D 58, 116002 (1998).
- [14] V. A. Kostelecký, Phys. Rev. D 69, 105009 (2004).
- [15] Q. G. Bailey and V. A. Kostelecký, Phys. Rev. D 74, 045001 (2006).
- [16] V. A. Kostelecký and J. D. Tasson, Phys. Rev. D 83, 016013 (2011)
- [17] V. A. Kostelecký and M. Mewes, Phys. Lett. B 779, 136 (2018).
- [18] O. W. Greenberg, Phys. Rev. Lett. 89, 231602 (2002).
- [19] V. A. Kostelecký and N. Russell, Rev. Mod. Phys. 83, 11 (2011).
- [20] A. Hees, Q.G. Bailey, A. Bourgoin, H.P. -L. Bars, C. Guerlin, and C. Le Poncin-Lafitte, Universe 2, 30 (2016).
- [21] L. Shao and N. Wex, Sci. China Phys. Mech. Astron. 59, 699501 (2016).
- [22] V. A. Kostelecký and M. Mewes, Phys. Lett. B **766**, 137 (2017).
- [23] C.-G. Shao et al., Phys. Rev. Lett. 117, 071102 (2016).
- [24] Q. G. Bailey, Phys. Rev. D 94, 065029 (2016).
- [25] Q. G. Bailey and D. Havert, Phys. Rev. D 96, 064035 (2017).
- [26] R. Bluhm, Phys. Rev. D 91, 065034 (2015).
- [27] J. B. R. Battat, J. F. Chandler, and C. W. Stubbs, Phys. Rev. Lett. **99**, 241103 (2007).
- [28] A. Bourgoin, C. Le Poncin-Lafitte, A. Hees, S. Bouquillon, G. Francou, and M.-C. Angonin, Phys. Rev. Lett. 119, 201102 (2017).
- [29] H. Mueller, S.-w. Chiow, S. Herrmann, S. Chu, and K.-Y. Chung, Phys. Rev. Lett. **100**, 031101 (2008).
- [30] K.-Y. Chung, S.-w. Chiow, S. Herrmann, S. Chu, and H. Mueller, Phys. Rev. D 80, 016002 (2009).
- [31] N. A. Flowers, C. Goodge, and J. D. Tasson, Phys. Rev. Lett. 119, 201101 (2017).
- [32] V. A. Kostelecký and J. D. Tasson, Phys. Lett. B 749, 551 (2015).
- [33] L. Shao and N. Wex, Classical Quantum Gravity 29, 215018 (2012).
- [34] L. Shao, R. N. Caballero, M. Kramer, N. Wex, D. J. Champion, and A. Jessner, Classical Quantum Gravity 30, 165019 (2013).
- [35] L. Shao, Phys. Rev. Lett. 112, 111103 (2014).
- [36] L. Shao, Phys. Rev. D 90, 122009 (2014).
- [37] Y. Xie, in *Proceedings of IAU Symposium 291—Neutron Stars and Pulsars: Challenges and Opportunities after 80*

- years (Beijing, China) (Cambridge University Press, Cambridge, 2013), Vol. 291, p. 558.
- [38] L. Shao, Universe 2, 29 (2016).
- [39] A. Hees, Q. G. Bailey, C. Le Poncin-Lafitte, A. Bourgoin, A. Rivoldini, B. Lamine, F. Meynadier, C. Guerlin, and P. Wolf, Phys. Rev. D 92, 064049 (2015).
- [40] B. P. Abbott *et al.* (Virgo, LIGO Scientific Collaborations), Phys. Rev. Lett. **119**, 161101 (2017).
- [41] B. P. Abbott *et al.* (Virgo, Fermi-GBM, INTEGRAL, LIGO Scientific Collaborations), Astrophys. J. **848**, L13 (2017).
- [42] Q. G. Bailey, A. Kostelecký, and R. Xu, Phys. Rev. D 91, 022006 (2015).
- [43] C.-G. Shao, Y.-F. Chen, Y.-J. Tan, J. Luo, S.-Q. Yang, and M. E. Tobar, Phys. Rev. D 94, 104061 (2016).
- [44] T. Damour and G. Esposito-Farèse, Phys. Rev. Lett. 70, 2220 (1993).
- [45] L. Shao, N. Sennett, A. Buonanno, M. Kramer, and N. Wex, Phys. Rev. X 7, 041025 (2017).
- [46] V. A. Kostelecký and M. Mewes, Phys. Lett. B 757, 510 (2016).
- [47] V. A. Kostelecký and S. Samuel, Phys. Rev. D 40, 1886 (1989).
- [48] B. A. Jacoby, P. B. Cameron, F. A. Jenet, S. B. Anderson, R. N. Murty, and S. R. Kulkarni, Astrophys. J. 644, L113 (2006).
- [49] S. M. Carroll, J. A. Harvey, V. A. Kostelecký, C. D. Lane, and T. Okamoto, Phys. Rev. Lett. 87, 141601 (2001).
- [50] R. Gambini and J. Pullin, Phys. Rev. D **59**, 124021 (1999).
- [51] C. M. Will, Theory and Experiment in Gravitational Physics (Cambridge University Press, Cambridge, England, 1993).
- [52] T. Damour and J. H. Taylor, Phys. Rev. D 45, 1840 (1992).
- [53] S. M. Kopeikin, Astrophys. J. Lett. 467, L93 (1996).
- [54] D. R. Lorimer and M. Kramer, *Handbook of Pulsar Astronomy* (Cambridge University Press, Cambridge, England, 2005).
- [55] J. M. Weisberg and Y. Huang, Astrophys. J. 829, 55 (2016).
- [56] E. Fonseca, I. H. Stairs, and S. E. Thorsett, Astrophys. J. 787, 82 (2014).
- [57] M. Kramer et al., Science 314, 97 (2006).
- [58] J. Antoniadis et al., Science **340**, 1233232 (2013).
- [59] P. C. C. Freire, N. Wex, G. Esposito-Farèse, J. P. W. Verbiest, M. Bailes, B. A. Jacoby, M. Kramer, I. H. Stairs, J. Antoniadis, and G. H. Janssen, Mon. Not. R. Astron. Soc. 423, 3328 (2012).
- [60] K. Lazaridis et al., Mon. Not. R. Astron. Soc. 400, 805 (2009).
- [61] G. Desvignes et al., Mon. Not. R. Astron. Soc. 458, 3341 (2016).
- [62] R. D. Ferdman et al., Astrophys. J. 711, 764 (2010); 713, 710 (2010).
- [63] Z. Arzoumanian et al., Astrophys. J. Suppl. Ser. 235, 37 (2018).
- [64] C. Lange, F. Camilo, N. Wex, M. Kramer, D. C. Backer, A. G. Lyne, and O. Doroshenko, Mon. Not. R. Astron. Soc. 326, 274 (2001).
- [65] N. Wex, in *Frontiers in Relativistic Celestial Mechanics: Applications and Experiments*, edited by S. M. Kopeikin (Walter de Gruyter GmbH, Berlin/Boston, 2014), Vol. 2, p. 39.
- [66] G. Hobbs, Classical Quantum Gravity **30**, 224007 (2013).

- [67] M. Kramer and D. J. Champion, Classical Quantum Gravity 30, 224009 (2013).
- [68] M. A. McLaughlin, Classical Quantum Gravity 30, 224008 (2013).
- [69] J. M. Weisberg, D. J. Nice, and J. H. Taylor, Astrophys. J. 722, 1030 (2010).
- [70] N. Wex and M. Kramer, Mon. Not. R. Astron. Soc. 380, 455 (2007).
- [71] M. Kramer, Int. J. Mod. Phys. D 25, 1630029 (2016).
- [72] N. Sennett, L. Shao, and J. Steinhoff, Phys. Rev. D 96, 084019 (2017).
- [73] C. Patrignani *et al.* (Particle Data Group), Chin. Phys. C 40, 100001 (2016).
- [74] V. A. Kostelecký and J. Tasson, Phys. Rev. Lett. 102, 010402 (2009).
- [75] V. A. Kostelecký and M. Mewes, Phys. Rev. Lett. 99, 011601 (2007).

- [76] V. A. Kostelecký and M. Mewes, Phys. Rev. D 80, 015020 (2009).
- [77] C. M. Will, Astrophys. J. 185, 31 (1973).
- [78] G. Gibbons and C. M. Will, Stud. Hist. Phil. Sci. B 39, 41 (2008).
- [79] L. Shao and N. Wex, Classical Quantum Gravity 30, 165020 (2013).
- [80] L. Shao, Classical Quantum Gravity **34**, 175011 (2017).
- [81] R. Nan, D. Li, C. Jin, Q. Wang, L. Zhu, W. Zhu, H. Zhang, Y. Yue, and L. Qian, Int. J. Mod. Phys. D 20, 989 (2011).
- [82] L. Shao et al., Proc. Sci., AASKA14 (2015) 042.
- [83] M. Kramer, D. C. Backer, J. M. Cordes, T. J. W. Lazio, B. W. Stappers, and S. Johnston, New Astron. Rev. 48, 993 (2004).